Natural climate variability is an important aspect of future projections of snow water resources and rain-on-snow events

Michael Schirmer[1,2], Adam Winstral[2†], Tobias Jonas[2], Paolo Burlando[3], Nadav Peleg[3,4]

[1]Swiss Federal Institute for Forest, Snow and Landscape Research, 8903 Birmensdorf, Switzerland
5 [2]WSL Institute for Snow and Avalanche Research SLF, 7260 Davos, Switzerland
[†] Deceased in March, 2021
[3]Institute of Environmental Engineering, ETH Zurich, 8093 Zurich, Switzerland
[4]Institute of Earth Surface Dynamics, University of Lausanne, 1015 Lausanne, Switzerland

Correspondence to: Michael Schirmer (michael.schirmer@wsl.ch)

10 **Abstract.**

Climate projection studies of future changes in snow conditions and resulting rain-on-snow (ROS) flood events are subject to large uncertainties. Typically, emission scenario uncertainties and climate model uncertainties are included. This is the first study on this topic to also include quantification of natural climate variability, which is the dominant uncertainty for precipitation at local scales with large implications for e.g. runoff projections. To quantify natural climate variability, a weather 15 generator was applied to simulate inherently consistent climate variables for multiple realizations of current and future climates at 100 m spatial and hourly temporal resolution over a 12 x 12 km high-altitude study area in the Swiss Alps. The output of the weather generator was used as input for subsequent simulations with an energy balance snow model. The climate change signal for snow water resources stands out as early as mid-century from the noise originating from the three sources of uncertainty investigated, namely uncertainty in emission scenarios, uncertainty in climate models, and natural climate 20 variability. For ROS events, a climate change signal toward more frequent and intense events was found for an RCP 8.5 scenario at high elevations at the end of the century, consistently with other studies. However, for ROS events with a substantial contribution of snowmelt to runoff (>20%), the climate change signal was largely masked by sources of uncertainty. Only those ROS events where snowmelt does not play an important role during the event will occur considerably more frequently in the future, while ROS events with substantial snowmelt contribution will mainly occur earlier in the year but not more 25 frequently. There are two reasons for this: first, although it will rain more frequently in midwinter, the snowpack will typically still be too cold and dry and thus cannot contribute significantly to runoff; second, the very rapid decline in snowpack toward early summer, when conditions typically prevail for substantial contributions from snowmelt, will result in a large decrease in ROS events at that time of the year. Finally, natural climate variability is the primary source of uncertainty in projections of ROS metrics until the end of the century, contributing more than 70% of the total uncertainty. These results imply that both 30 the inclusion of natural climate variability and the use of a snow model, which includes a physically-based processes representation of water retention, are important for ROS projections at the local scale.

1   Introduction

The future decrease of snow depth and snow water equivalent in mountainous environments due to global warming has been
35   shown in several studies (e.g. Musselman et al., 2017; Marty et al., 2017; Verfaillie et al., 2018, Willibald et al., 2020). The
frequency and intensity of rain-on-snow (ROS) events are also foreseen to alter due to changes in the snow cover, the
precipitation phase, and the rain frequency and intensity (e.g. Beniston and Stoffel, 2016). Despite a decreasing snow cover,
ROS events have been predicted to become more frequent and intense at high elevations (Surfleet and Tullos, 2013; Beniston
and Stoffel, 2016; Morán-Tejeda et al., 2016; Musselman et al., 2018; Ohba and Kawase, 2020; Sezen et al., 2020). Different
40   sources of uncertainty were considered in some of these studies, however, none of them have included internal climate
variability in their analysis.

The latter is largely a consequence of the chaotic nature of the atmosphere (Deser et al., 2012a). It is a result of purely periodic
external forcing, non-linear interplay of feedbacks within the climate system and random fluctuations in physical or chemical
factors in the atmosphere (Ghil, 2002). For climate change analyses, the role of internal climate variability on projections of
45   air temperature and precipitation has been quantified together with other uncertainty sources, e.g. emission scenario and
climate model uncertainty (Hawkins and Sutton, 2009; 2011; Deser et al., 2012b, Fatichi et al., 2016). In general, the smaller
the scale and the shorter the time horizon of the projections, the more important is the relative contribution of internal climate
variability to overall uncertainty (e.g. Hawkins and Sutton, 2011). Projections of precipitation are generally more affected by
natural climate variability than those of air temperature (Hawkins and Sutton, 2009; 2011; Peleg et al., 2019). For mean and
50   extreme precipitation at local scales (i.e. weather stations) internal climate variability is the dominant source of uncertainty,
not only for short time horizons but also through the end of this century (Fatichi et al., 2016). While it is possible for future
research to reduce the amount of uncertainty if climate models are improved or emission scenarios are constrained, the amount
of natural climate variability is not reducible. These findings raise the question of how informative climate projections based
only on climate model outputs are and will be at local scales (Fatichi et al., 2016).

55   Willibald et al. (2020) studied the effects of internal climate variability on the change of mean and maximum snow depth at
eight stations in the Swiss Alps and concluded that it is a major source of uncertainty for time horizons up to 50 years and
more. For a high elevated station (Weissfluhjoch, 2540 m a.s.l.) they found no significant trends for maximum snow depth in
80% of 50 realizations of future climate periods for a 50-year period, and no significant trends in 20% of the realizations for a
period up to the end of the century. The effects of internal climate variability on projected runoff have been highlighted in
60   several studies. For instance, the climate change signals for the mean, frequency, and seasonality of runoff in the middle of
this century are masked by natural climate variability (Fatichi et al., 2014), while it will emerge by the end of the century
(Addor et al., 2014). The signal varies with elevation and is dependent on the hydrological components (e.g. snowmelt,
evapotranspiration) that drives the runoff (Moraga et al., 2021). Lafaysse et al. (2014) concluded that internal climate
variability is capable of exacerbating, moderating, or even reversing a climate change signal of streamflow. These studies

65   indicate the importance of including internal climate variability in studies of climate change impacts on catchment-scale hydrologic response.

In this study, the uncertainty of future projection of snow water resources and rain-on-snow characteristics at local scales were quantified in relation to natural climate variability, climate model and scenario uncertainty at the local scale. We hypothesize that snow water resources are less affected by internal climate variability than rainfall-driven runoff because they are more

70   dependent on air temperature. We will show for which time horizon (e.g. for projections for mid and end of the century) and emission scenario the signal of change in snow water equivalent (SWE) amounts is not masked by internal climate variability. The frequency and intensity of ROS events are hypothesized to be more influenced by natural precipitation variations compared to SWE, as they may be less dependent on air temperature. We will explore whether the commonly found increase in ROS frequency and intensity hold for future climates when natural climate variability is considered. To this end we used simulations

75   of a high-resolution weather generator, AWE-GEN-2D, generating multiple stochastic ensembles of future climate projections that have been shown to realistically represent natural climate variability (Peleg et al., 2017). To account for the complexity of snow accumulation and melt processes and their response to a changing climate (in line with the discussion in Clark et al., 2016) we used in our analysis an energy balance snow model at high spatial and temporal resolution.

2   Methods

80   ### 2.1   Study area

The "Gletsch" area in central Switzerland, with altitudes between 1400 and 3500 m a.s.l. and with an extent of 144 km^2 (Fig. 1), has been selected as the study area. It has a mean annual air temperature of -1.3°C and a mean annual precipitation of 1700 mm. Nival conditions prevail at these elevations today, yet the area is low enough that climate change may affect the current snow regime (e.g. Marty et al., 2016). The study area was chosen to encompass the elevation range for which an increase in the

85   number of ROS events has been shown in other studies. Observational data for training the weather generator and validating the model chain in and near the study area were available as detailed in Table 1. Note that the Rhone glacier is located within the study area, but its receding effect was not considered because only seasonal snow was of interest in this study.
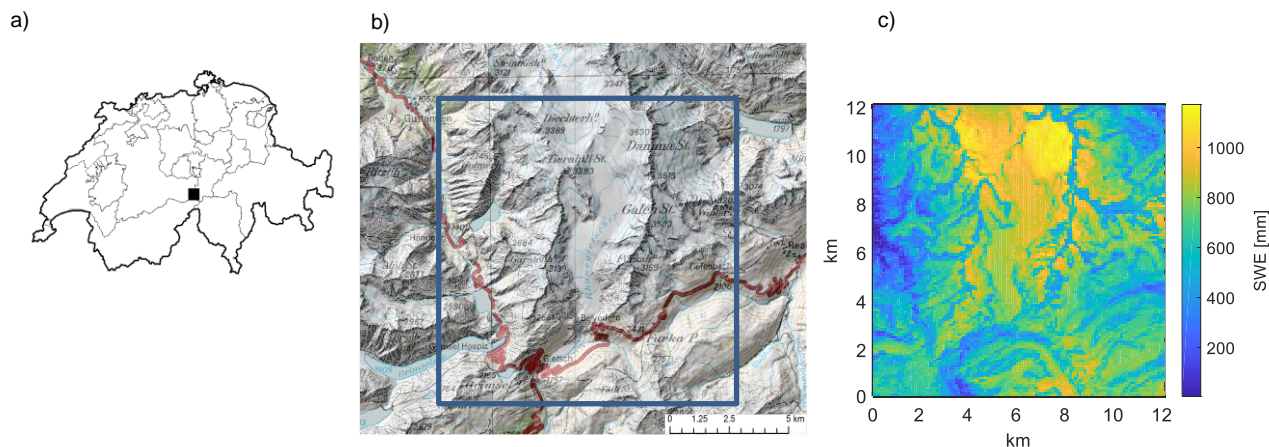
Figure 1. Location of the study area in Switzerland (46.56° N, 8.36° E, WGS 84) (a) and map showing the extent of the model domain (source: Federal Office of Topography swisstopo) (b). Example of modeled SWE at April 1 of a random year during current climate conditions (c).

2.2 Snow model

The snow model used in this study is an energy balance snow model, an evolution of the Jules Investigation Model (JIM; Essery, 2013). Only a single model configuration from this multi-model framework was used, determined by comparison against comprehensive datasets including snow lysimeter data (Magnusson et al., 2015). This model was advanced by integrating a seasonal algorithm for the fraction of snow-covered area (Helbig et al., 2015; 2021), a sub-grid precipitation adjustment that implicitly accounts for preferential deposition and avalanches using LiDAR data, and a local calibration of the albedo routine that better reflects the observed variability of the albedo decrease rate in Switzerland (not published). This model setup is used for the Operational Snow Hydrological Service in Switzerland to predict snowmelt runoff and has been thoroughly developed through several studies (Griessinger et al., 2019; Winstral et al., 2019; Helbig et al., 2021). The snow model requires total precipitation (Precip), air temperature (TA), incoming shortwave radiation (ISWR), incoming longwave radiation (ILWR), wind, air pressure and relative humidity in an hourly resolution. Precipitation was split into solid and liquid phases using an adaptation of the method presented in Magnusson et al. (2014) originally developed for daily data.

2.3 Weather generator

The AWE-GEN-2D model (Peleg et al., 2017) was used to stochastically generate gridded climate variables for the study area at 100 m spatial and hourly temporal resolution. The model was developed to simulate climate variables in complex terrain by combining physical and stochastic-statistical methods that enable preserving physical and observed dependencies between climate variables. This combination provides the necessary computational efficiency to generate a multiplicity of climate periods to analyze the influence of natural variability. This weather generator is capable of reproducing both principal statistics and natural climate variability for those climate variables needed for subsequent energy balance snow modeling (Peleg et al.,

2017). It requires observational data for calibration, which are summarized in Table 1. Spatial fields of total annual precipitation were created specifically for this study with optimal interpolation (OI) of snow depth sensor data and a gridded precipitation product, RhiresD (Scharb, 2000; MeteoSwiss, 2019), using a >20-year data set following the procedures detailed in Magnusson et al. (2014). This method corrects for undercatch in snowfall data, a typical problem of mountainous regions. The wind speed was spatially adjusted to match the debiased wind speeds of a numerical weather prediction model in this region (Winstral et al., 2017). For future climate conditions, the weather generator is reparametrized using a factor of change approach that requires the output of climate models (Peleg et al., 2019). For this study, a spatial resolution of 100 m was chosen to account for small-scale processes that are imperative for capturing the spatial variability of snowmelt dynamics in small mountain catchments (e.g. terrain shading of direct radiation). A resolution of 1 km was chosen for precipitation but simulations were subsequently linearly resampled to 100 m. The model domain consists of 120 x 120 grid points. 50 realizations of 30 years each, representing the same climatic period, were used to explore the natural climate variability. This is consistent with the setup presented by Peleg et al. (2017; 2019).

In summary, the weather generator was used to (1) downscale and debias regional climate model output, (2) provide hourly data, (3) generate the full set of required inputs for the energy balance snow model, (4) generate climate variables with intervariable consistency, and (5) generate multiple realizations of current and future climate periods.

Table 1. Overview of observational data used for calibration and validation. The italic inputs are weather stations either within or with shown distance to the study area. TA is air temperature, RH is relative humidity, ISWR is incoming shortwave radiation, ILWR is incoming longwave radiation, Precip is total precipitation, and HS is snow depth.

Input	Variable	Calibration purpose	Distance in km
Calibration			
Grimsel Hospiz (1980 m)	Precip	(Inter-)Storm duration	0
Engelberg (1036 m)	TA	TA lapse rate	18
Titlis (3040 m)	TA	TA lapse rate	13
Grimsel Hospiz (1980 m)	TA, RH, ISWR	TA lapse rate, vapour pressure	0
Weather radar	Precip	mean areal rainfall, wet area ratio	
Merra reanalysis		cloud area ratio	
Optimal interpolated fields	Precip	Monthly mean rainfall	
Validation			
Grimsel Hospiz (GRH, 1980 m)	TA, ISWR, ILWR		0
Guetsch (GUE, 2286 m)	HS		13
Oberwald 1 (OBW1, 2733 m)	TA		0
Oberwald 2 (OBW2, 2432 m)	HS		0

2.4 Climate models

130 Regional climate models from the EURO-CORDEX archive (Jacob et al., 2014) were used to obtain the CH2018 climate
scenarios (CH2018 Project Team, 2018), which was used in this study to calculate factors of change (FC) (Anandhi et al.,
2011) needed for the downscaling procedure (cp. Sect. 2.2). The FC consist of gridded values downscaled to 2-km resolution
using quantile mapping (CH2018 Project Team, 2018). Only the 10 EURO-CORDEX model chains with the highest spatial
resolution of 11 km were used (Table S1). The FC were calculated for two emission scenarios (i.e. RCP 4.5 and RCP 8.5) and
135 two time horizons (i.e. a mid-century period from 2030 to 2059 and an end-of-century period from 2070 to 2099). Finally, FC
were linearly interpolated to our 100 m resolution.

2.5 Quantification of climate change in relation to uncertainty sources

For the sake of consistency, we compared only simulated values of current and future climates without analyzing climate-
related changes between the model and observed data. However, the model was verified against observed data under current
140 climate conditions in Sect. 3.1. Climate period mean values of 50 and 500 (i.e. 50 realizations times ten climate models) of
simulated current and future climate periods, respectively, were analyzed. The 5-95th percentile range of the 50 (500) climate
period mean values was chosen to quantify natural climate variability (and climate model uncertainty for future climate
conditions, respectively), consistent with other studies (e.g. Fatichi et al., 2016; Peleg et al., 2019). Note that this procedure
does not quantify the natural interannual variability (e.g. a high snow year vs. a low snow year), but how different entire
145 climate periods are (e.g. a high snow climate period vs. a low snow climate period).

2.6 Uncertainty partitioning

To obtain the relative contribution of the investigated sources of uncertainty (i.e. natural climate variability, climate model
uncertainty, and emission scenario uncertainty) to the total uncertainty, the partitioning method presented by Fatichi et al.
(2016) was applied. Separately for the two time horizons and the two emission scenarios, a climate change signal was computed
150 for each variable (e.g. SWE or ROS frequency) as the difference between the mean of a future and a current climate period
determined from the stochastic realizations. Note that the 50 realizations of the climate periods are completely random,
meaning that, for example, the first current climate period and the first future climate period have no stochastic similarities.
Climate model uncertainty was calculated using the median of 50 realizations of this climate change signal and then quantified
using the 5-95th percentile range across the ten climate model chains (i.e. the minimum and maximum) for each emission
155 scenario and for each period. The average range of both emission scenarios is then considered to be the total climate model
uncertainty. For natural climate variability, the 5-95th percentile range of the 50 realizations of the median climate change
signal from all climate model chain was calculated. Similarly to total climate uncertainty, the total natural climate variability
is the average range of both emission scenarios. For the emission scenario uncertainty, the median was calculated for both
emission scenarios over all of the 500 climate change signal values (10 climate model chains and 50 realizations of climate

160   periods). The emission scenario uncertainty is then the difference between the two median values. Finally, the total uncertainty
was calculated with the 5-95th percentile range over all of the 1000 change signals resulting from 10 climate models, 50
realizations of climate periods, and two emission scenarios.

For the fractional uncertainties, the sources of uncertainty were scaled by the total uncertainty. In the case of SWE, this value
is available for each day and is then averaged into a weighted annual value: the daily total uncertainty values were used as
165   weights to avoid overweighting days with only low climate change signal uncertainty (e.g. at the beginning and end of the
season).

Note that individual sources of uncertainty do not have to sum to one, as they do for variances of uncorrelated random variables:
here a range of percentiles were considered, not a variance (see further discussion in Fatichi et al., 2016). Possible correlations
between sources of uncertainty were not examined here.

170   **2.7   Rain-on-snow definition**

Based on the high-resolution results, a "contributing area" of a ROS event can be defined. This procedure realistically describes
the elevation-dependent effects on the phase of the precipitation in combination with the presence and condition of the
snowpack. For a single ROS event, these parameters vary in space, i.e. they delineate an area of varying size that contributes
significantly to a ROS event ("contributing area"). Four pixel-based criteria were applied for daily values to define a
175   contributing area, which can be found in Table 2. The criteria differ in the amount of daily rainfall, and whether there is a
substantial contribution of snowmelt to surface water input (SWI) or not. Snowmelt is defined here as SWI minus rainfall, i.e.
the portion of surface water input that comes from the melting process. Note that criterion 1 in Table 2 is the same as that of
Musselman et al. (2018).

180   **Table 2. Four alternative pixel-based criteria for ROS events.**

Criterion	SWE [mm]	Rain [mm/d]	Snowmelt [%SWI]
1	>10	>10	> 20
2	>10	>10	-
3	>10	>20	> 20
4	>10	>20	-

3   Results and Discussion

3.1   Verification

3.1.1   Weather generator

185   Peleg et al. (2017) showed for a nearby mountainous region that the weather generator can reproduce principle statistics of climate variables. For this study, a similar verification to Peleg et al. (2017) was conducted. For annual precipitation, a similar quality was achieved compared to Peleg et al. (2017), as is expected since monthly mean values are used for calibration (not shown). Figure 2 shows a comparison for air temperature (TA), incoming shortwave radiation (ISWR), and incoming longwave radiation (ILWR) with measured data at two stations in the study area. Note that for Grimsel Hospiz (GRH), ISWR was

190   indirectly used for calibration of the weather generator. Specifically, the data were used to calibrate the vapor pressure, but not for the variable itself. It should also be noted that the data availability for the stations spans only a few years and may not represent the long-term distribution well. Apart from these limitations, it can be seen that TA is slightly colder at the lower station OBW2 in AWE-GEN-2D (bias of -0.8 °C), while it is quite well represented at the higher station OBW1. ISWR is underestimated in winter months, while ILWR is overestimated in spring. However, it is our understanding that the quality of

195   the output is sufficient to analyze deviations of simulated future climate conditions from current ones, i.e. no climate-related changes are compared between the model and observed data. Note that the range plotted is inter-year variability, in contrast to Sect. 3.2 and following, where inter-climate period variability is discussed.
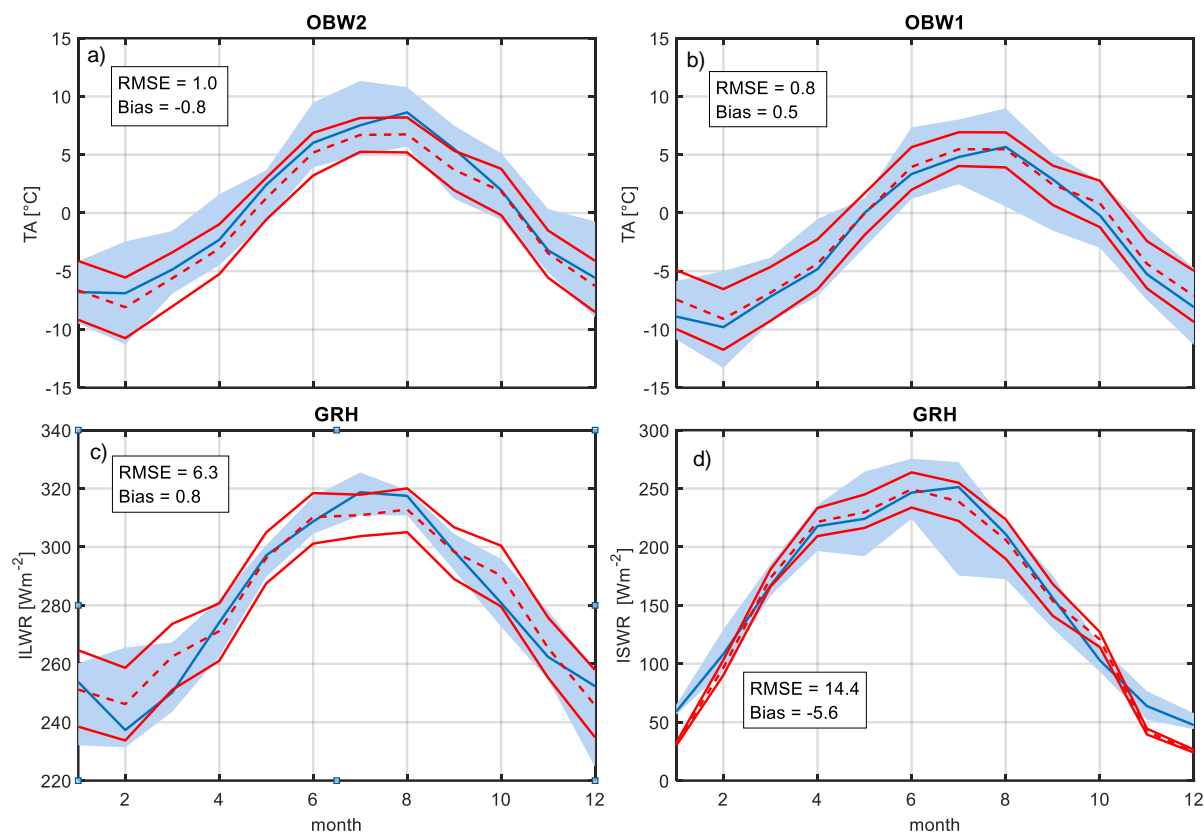
Figure 2. Monthly mean values for air temperature (TA) (a) and (b), incoming shortwave radiation (ISWR) (c), incoming longwave radiation (ILWR) (d) at the stations Oberwald 1 and 2 (OBW1, 2), and Grimsel Hospiz (GRH). Plotted are 5, 50 and 95th percentiles of observations in blue of 8 years (GRH) and 20 years (OBW1, 2), and modeled data in red of 1500 years. RMSE and Bias are calculated for 50ᵗʰ percentiles.

3.1.2   Snow model

Recent publications demonstrate the quality of point-based snow depth modeling (Winstral et al., 2019), of spatial modelling results as inputs to a hydrologic runoff model (Griessinger et al., 2019), or in comparison to LiDAR-derived snow depth (HS) data and satellite-derived snowpack fraction data (Helbig et al., 2021). Using only measured station data as meteorological forcing, Magnusson et al. (2015) have already quantified the quality of the original JIM models with lysimeter data. In addition to these results, it is shown here that the improved model can accurately reproduce snow depth at the GUE station near the study area (Fig. 3). This station is located at 2286 m a.s.l. at about 13 km from the study area (see Table 1) and provides all required meteorological input data for energy balance snow modeling without major gaps and in good quality during the last two years. Except for precipitation, all input data were used without any preprocessing. For precipitation, a method similar to that used to train the weather generator using optimal interpolation was chosen (Magnusson et al., 2014, see Sect. 2.2). Since optimal interpolation is not able to handle structural biases (i.e. site-specific undercatch in the background field), a correction factor of 1.3 was chosen to correct for local undercatch and achieve better HS comparison during accumulation phases. With

this meteorological input, the ablation and settling behavior of the snow model could be assessed and good agreement was achieved in the two years studied, with a RMSE of 20 cm and a positive bias of 13 cm, calculated for days when either the model or the observations show positive snow depth (Fig. 3).

220
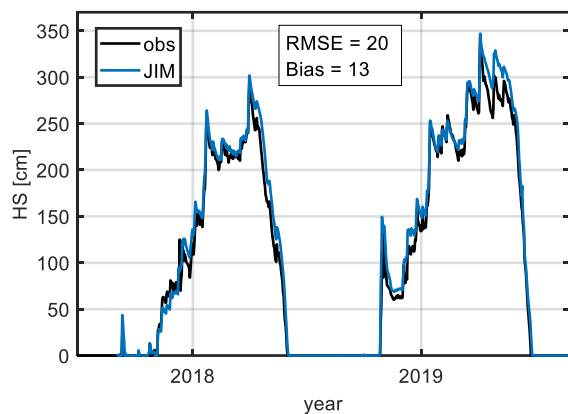
Figure 3. HS observed (obs) and modeled (JIM) with station input at station GUE.

3.1.3 Combined verification

To demonstrate that the combined model chain is capable of providing reasonable HS and SWE values, we compared these values at the grid cell where observed HS data and modeled SWE from the OBW 2 station are available (Fig. 4). Modeled SWE was determined using measured HS and a parametric model (HS2SWE) that accumulates, compacts, and melts snow layer by layer (Magnusson et al., 2014). Mean values and spread of 1500 years simulated by the model chain and (pseudo) observations of 20 years show good agreement. This indicates that the model chain is capable of reproducing both the interannual variability and mean properties. The comparison shows, however, a slight underrepresentation of years with early intense snowfall. Note that the range in the case of the observations is determined by minimum and maximum, compared to the 5-95th percentiles of the generated data. In addition, the model typically simulates an earlier onset of melting and subsequent slower melting is typically modeled, which compensates and finally results in a mean melt out that is consistent with observations. These small inconsistencies notwithstanding, the results show a level of performance that does not compromise the use of the model combination to study the effects of climate change based on simulated current and future climate periods.
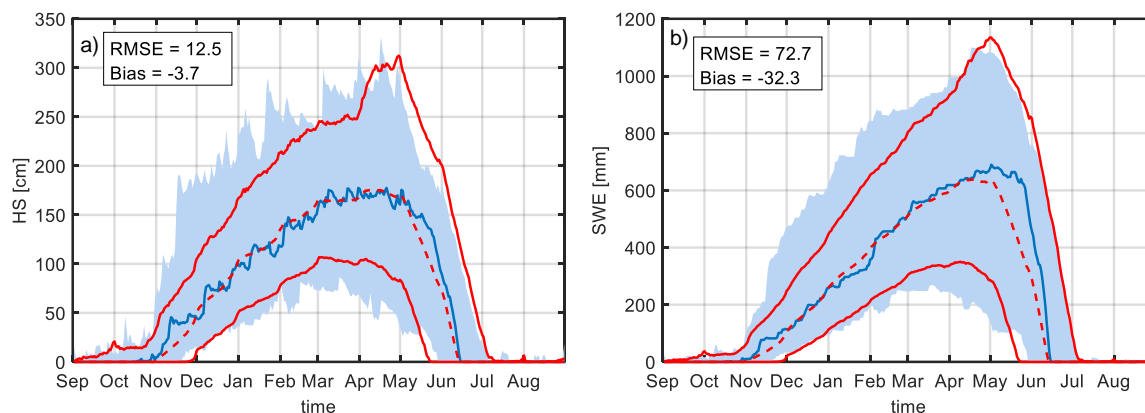
Figure 4. Snow depth measured (left) and SWE (right) determined by an HS2SWE model (blue) at station OBW 2. Plotted are the 5, 50 and 95 percentiles of 20 years of observations (blue) and 1500 years of weather-generator-snow-model data (red). RMSE and bias are calculated for 50 percentile values and for days when either the model or the observations show positive values.

3.2   Climate change impact

In this section, we first provide an overview of how natural climate variability and model uncertainty affect key inputs to snowpack modeling; second, we show projections of future seasonal SWE curves; third, we discuss changes in ROS properties; and finally, we provide a quantification of sources of uncertainty.

3.2.1   Natural climate variability and climate model uncertainty

Figure 5 shows the annual and spatial means of TA, precipitation, and SWE on April 1 for the current future climate conditions. Natural climate variability is shown with error bars, while climate model uncertainty can be interpreted with the differences between climate model chains. For TA, climate model uncertainty dominates, while for precipitation, natural climate variability dominates. This result is consistent with those presented in other studies (Hawkins and Sutton, 2009; 2011; Fatichi et al., 2016; Peleg et al., 2019). The total uncertainty range of SWE on April 1 is mainly generated by natural climate variability for the mid-century, while at the end of the century both sources of uncertainty contribute similarly. A more quantitative analysis of the specific uncertainty contributions can be found in Sect. 3.2.7. Note that all of the following figures show uncertainty ranges of climate period averages to illustrate how different equally likely realizations of a future climate period are. The inter-annual uncertainty range is much larger (not shown) and is not the subject of this paper.
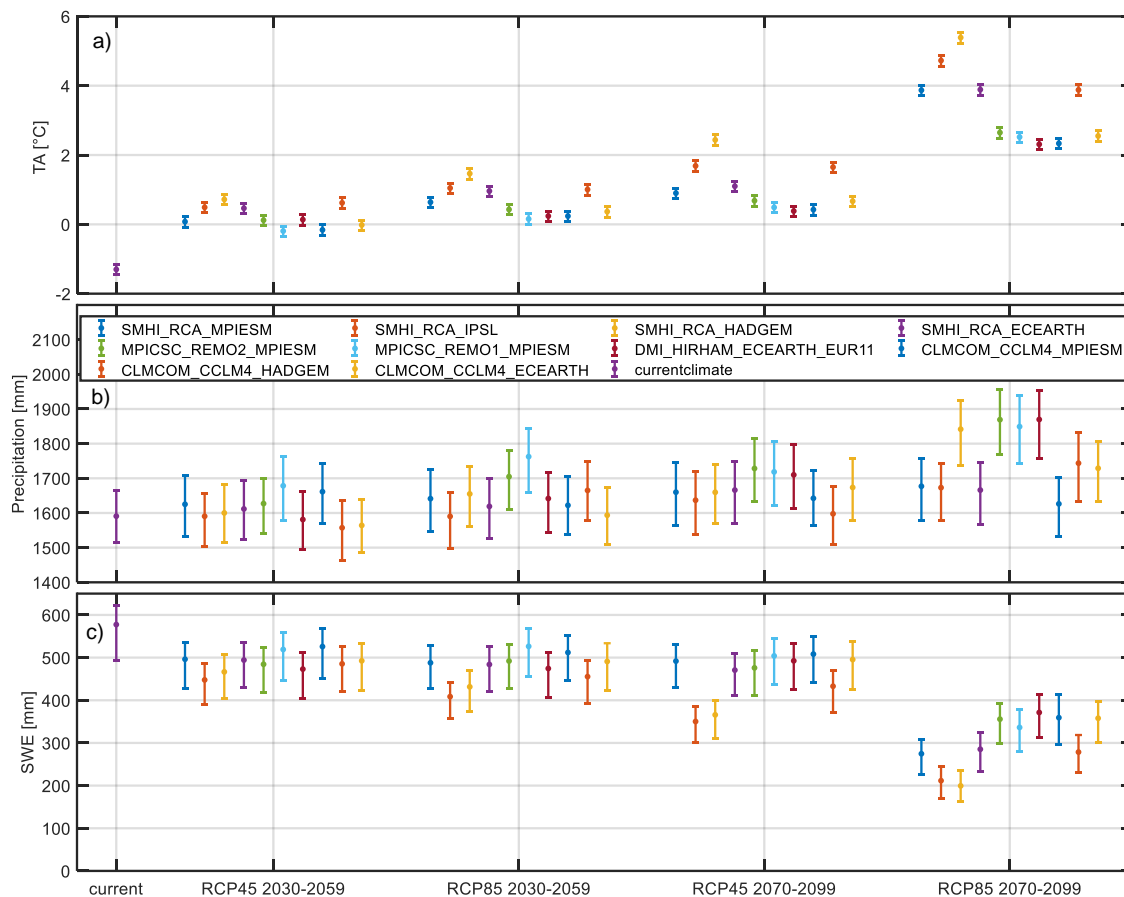
Figure 5. Natural variability and climate model uncertainty of annual and spatial mean precipitation, air temperature (TA) and resulting spatial mean SWE at April 1. Plotted are the 5, 50, 95 percentiles from 50 realizations of climate period mean values.

3.2.2 Change in seasonal SWE

Figure 6 shows the seasonal evolution of areal mean SWE for different emission scenarios and periods. The uncertainty range for current climate (blue) is, by definition, only determined by natural variability, while for future climate (red) it is influenced by a composite of natural variability and climate model uncertainty. From May on, the changes in SWE for all emission scenarios and time horizons are larger than the uncertainty range (i.e. no overlap of uncertainty ranges). During the accumulation period, only the extreme emission scenario RCP 8.5 at the end of the century shows no overlap, while overlaps of up to 50% are achieved for the other cases. At the time of the SWE maximum in this region (May 1st), the overlap is already close to zero due to the onset of melting in the future scenarios. Similar to Verfaillie et al. (2018), the uncertainty in the emission scenarios is only relevant at the end of the century, as discussed in detail in Sect. 3.2.7.

For all scenarios, the altitude effects are similar. At the lowest altitudes (1400 - 1950 m a.s.l.), the climate signal is large enough to emerge clearly from the uncertainty ranges, while the largest overlap is achieved at the highest altitudes (3050 - 3600 m a.s.l.) (Fig. S1). Only for the most extreme scenario, RCP 8.5 at the end of the century, no overlap is achieved even at the

270 highest altitude range. This is generally consistent with the results of Marty et al. (2017), who also found a weakening of the climate change signal at higher elevations. Furthermore, the results are mostly consistent with Willibald et al. (2020) who found a similar elevation effect in how natural climate variability can mask trends in mean and maximum snow depth, although, the role of natural climate variability seems to be larger in their study than in our results. While at a low altitude site only 15% of 50 realizations of future climate conditions under RCP 8.5 showed insignificant trends for time horizons until the mid of

275 the century, at a high-altitude site (Weissfluhjoch, 2540 m) it was still 80%. For the latter station, they still found 20% of all realizations with insignificant trends until the end of the century. For our data for RCP 8.5 at the end of the century, no overlap is found for SWE for no time of the year and also not for the highest altitude range. Also, for low elevations at the mid of the century, hardly any overlap is exhibited (Fig. S1a).

In summary, these results suggest that the climate change signal for area-averaged SWE is generally larger than uncertainty

280 (including maximum SWE amounts) in the future. Only for elevations above 2000 m and for the months between January and April there are likely realizations of future climate with an equal amount of SWE as today. These exceptions can be characterized as situations where precipitation variability can strongly influence SWE amounts, i.e. when most of the precipitation falls as snow and melt is negligible. However, the later onset of SWE accumulation in future climate prevents natural variability from being able to fully mask the climate change signal in the accumulation season, as is the case with

285 precipitation (Peleg et al., 2019) or runoff (Fatichi et al., 2014, Moraga et al., 2021).
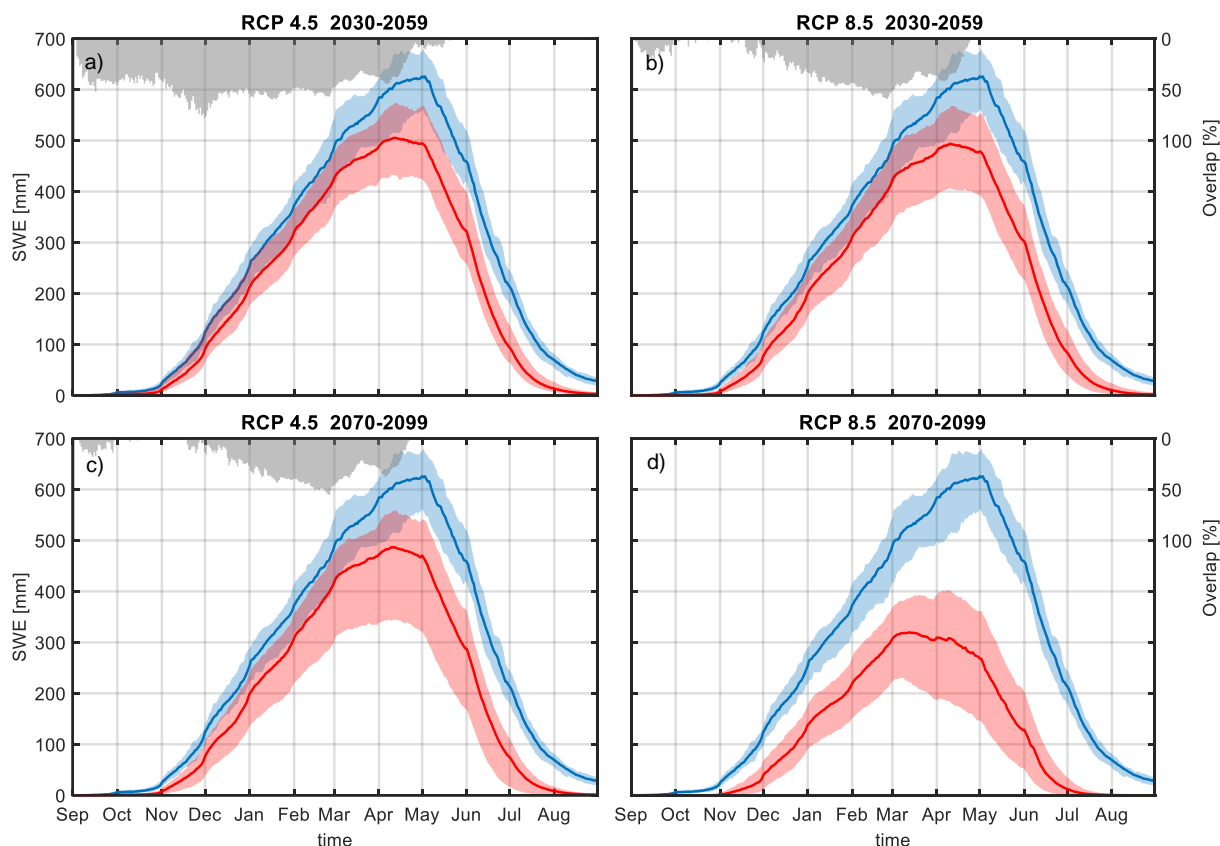
Figure 6. Areal mean seasonal SWE development under current (blue) and future climate (red) for different emission scenarios and time horizons. Plotted are the 5, 50, 95 percentiles of climate period mean values stemming from 50 (current climate) and 500 climate periods (future climate with 50 realizations of 10 climate models). The overlap indicates how much of the current climate natural variability is overlaid by the future climate uncertainty range.

3.2.3   Frequency of rain-on-snow events

presents the exceedance probability of contribution area sizes of ROS events for all different pixel-based criteria (see Table 2) for RCP 8.5 at the end of the century. For example, in Fig. 7a, using criterion 1, approximately nine ROS events per year (exceedance probability of 0.0247) are simulated with a contributing area greater than 20% of the total area for current and future climate conditions. For this most extreme scenario, there is a climate change signal toward more frequent events for most the contributing area size thresholds. However, whether or not the climate signal emerges from uncertainty ranges depends on the pixel-based criterion to define a ROS event. For criterion 4 and partially for criterion 2 (see Table 2) the signal of change is apparent, while it is not the case for criteria that also require 20% of the SWI contribution from snowmelt (criteria 1 and 3). Increasing the rainfall threshold results in a clearer climate change signal, likely because rainfall in higher precipitation intensities is more frequent at the end of the century (Fig. S2) due to more total precipitation (Fig. 5) and due to warmer air temperatures, which increase the liquid fraction. The reason why the increase in ROS frequency is masked when

the additional melt demand is used to define a ROS event can be found in the change of seasonality of ROS events and is discussed in Sect. 3.2.4. For other emission scenarios and ROS definitions, the overlap is even more pronounced (Fig. S3).

305
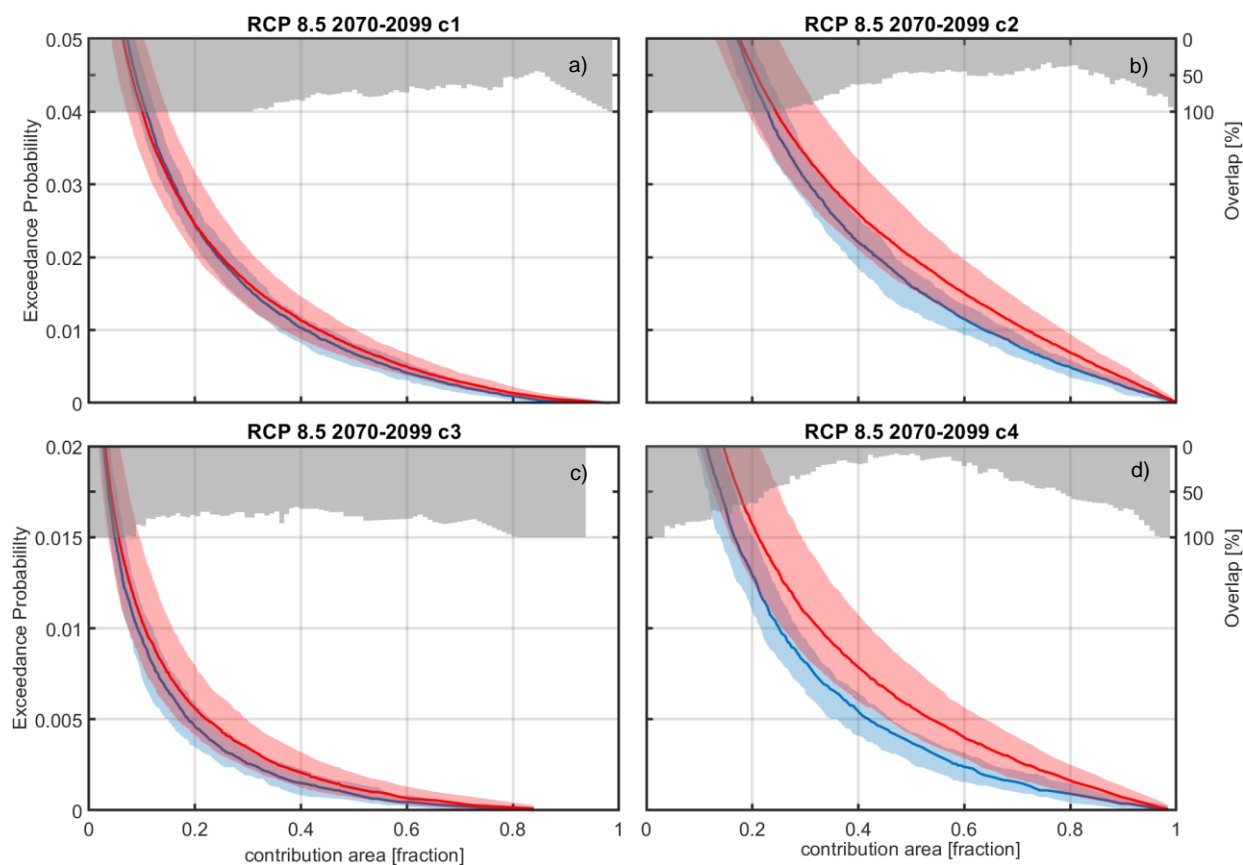
Figure 7. Yearly exceedance probability of contribution area size (as fraction of the total area) during ROS events for current climate (blue) and RCP 8.5 end of the century (red) for criteria 1 (c1) to 4 (c4). Plotted are the 5, 50, 95 percentiles of climate period mean values stemming from 50 (current climate) and 500 climate periods (future climate with 50 realizations of 10 climate models). The overlap indicates how much of the current climate natural variability is overlaid by the future climate uncertainty range.

310

It is also worth noting the altitude dependence of this analysis for RCP 8.5 at the end of the century. At high elevations typically above 2500 m a.s.l., the increase in ROS events is pronounced for criteria 2 (not shown) and 4 (Fig. S4). For all other criteria defining ROS events and all other emission scenarios and periods, an increase at high altitudes above 2500 m a.s.l. is also observed, but this is masked by the sources of uncertainty (e.g. Fig. S5 for criterion 1).

315 In summary, natural climate variability and climate model uncertainty question the claim that ROS events will become more frequent in a future climate in this high elevation study area, except for the most extreme scenario RCP 8.5 at the end of the century at high elevations above 2500 m if the ROS definition does not include a snowmelt contribution. If a ROS event is defined such that there must be a substantial snowmelt contribution (>20%), then a future increase in ROS frequency is masked by the sources of uncertainty included in this study without any exceptions.

320 Thus, our results confirm our initial hypothesis that ROS events are strongly influenced by natural climate variability because they are more driven by precipitation than by seasonal SWE curves. However, some studies do find an increase in ROS frequency at higher elevations (e.g. Beniston and Stoffel, 2016; Musselman et al. 2018), and a discussion on this can be found in Sect. 3.2.6.

3.2.4   Rain-on-snow seasonality

325 In this section, we discuss why the climate change signal is more pronounced for frequencies of ROS events with only minor snowmelt contribution versus substantial contribution. Following the definition of criterion 2, each ROS event can spatially consist of pixels that will also satisfy criterion 1, i.e. with snowmelt contribution > 20% to SWI (see Fig. S6 for a spatial example). Figure 8 shows in a histogram the number of ROS events per month and their spatial characteristic computed as the ratio φ of pixels obeying criterion 1 over pixels obeying criterion 2. During current climate conditions (Fig. 8a), most ROS

330 events occur from May to July, typically with large φ, i.e. a large spatial proportion of pixels with substantial snowmelt contribution. In January, for example, only a small number of ROS events occur, and most are characterized by a low φ, i.e. a small spatial proportion of pixels with substantial snowmelt contribution. This is consistent with the results of Würzer et al. (2016), who found that ROS events with a substantial snowmelt contribution typically occur in late spring and early summer, when the snowpack is wet and warm at the onset of the event. Conversely, a low snowmelt contribution is expected when the

335 initial snowpack is drier and colder (Würzer et al., 2016). Similar to Würzer et al. (2016), conditions for a substantial contribution from snowmelt are typically found under initially wet and warm snowpack conditions (Figs. 9a and b). This is indicated by the red arrow in Fig. 8, which points at large φ that is associated with typically wet and warm initial snowpack conditions.

340
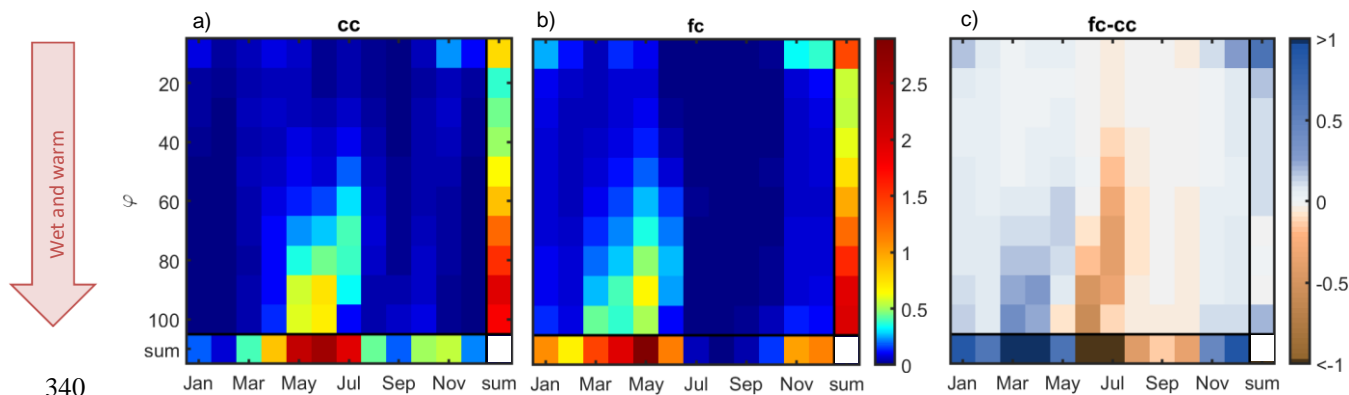
Figure 8. Histogram showing the number of ROS events for current climate (cc) (a) and future climate (fc) (b, RCP 8.5 at the end of the century), and the difference thereof (fc-cc) (c), split in different values of φ, i.e. the ratio of pixels obeying criterion 1 over pixels obeying criterion 2 per event. The colour bar indicates the number of ROS events per year averaged over 1500 years for the current climate and 10 x 1500 years for future climate conditions. For the month with the lowest number of ROS events in the current
345 **climate, in February, there are approximately 100 ROS events available in the data set.**

For RCP 8.5 at the end of the century (Fig. 8), the peak of ROS events shifts to earlier in the season, with typically large φ. There is also a higher number of early and midwinter events, with typically small spatial ratios, and almost no ROS events from July through September due to nonexistent snowpack.

The increase in ROS events in March and April with large φ values contrasts with a large decrease in June and July (Fig. 8c).
350 This means that the ROS events with spatially a large number of pixels with substantial snowmelt are not largely changing in the future with regards to their frequency, but rather shifted to earlier in the season. Only the frequency of events with small φ will increase in the future. This may be seen as counterintuitive at first because warm and wet conditions are expected to occur more frequently in a future climate state. Indeed, this is generally the case at the onset of ROS events (Figs. 9c and d). However, rain in early and midwinter will fall on snow that will – even in this extreme warming scenario – be typically too cold and too
355 dry to allow a significant contribution from snowmelt. This result implies that warmer air temperatures due to a changing climate can change the phase of precipitation more often than they can change the state of the snowpack to substantially contribute to runoff. This fact explains the limited increase in early and midwinter ROS events frequency with a large spatial proportion of substantially snowmelt contribution. Towards summer, the drastically reduced snow cover summer in a future climate explains the much faster decrease in the number of ROS events in this time, when ROS events have typically large φ,
360 compared to the current climate.

In summary, the occurrence of rain falling on an initially warm and wet snowpack will likely not increase in the future. This explains that the climate change signal of ROS frequency shown in Figs. 7a and c is masked by uncertainty sources, when a ROS event is defined by a substantial snowmelt contribution. However, a significant climate signal with varying signs is expected within individual months, e.g. March and June. These findings imply the need for a process-based snow model that
365 can adequately model snowpack retention, as shown in this study.
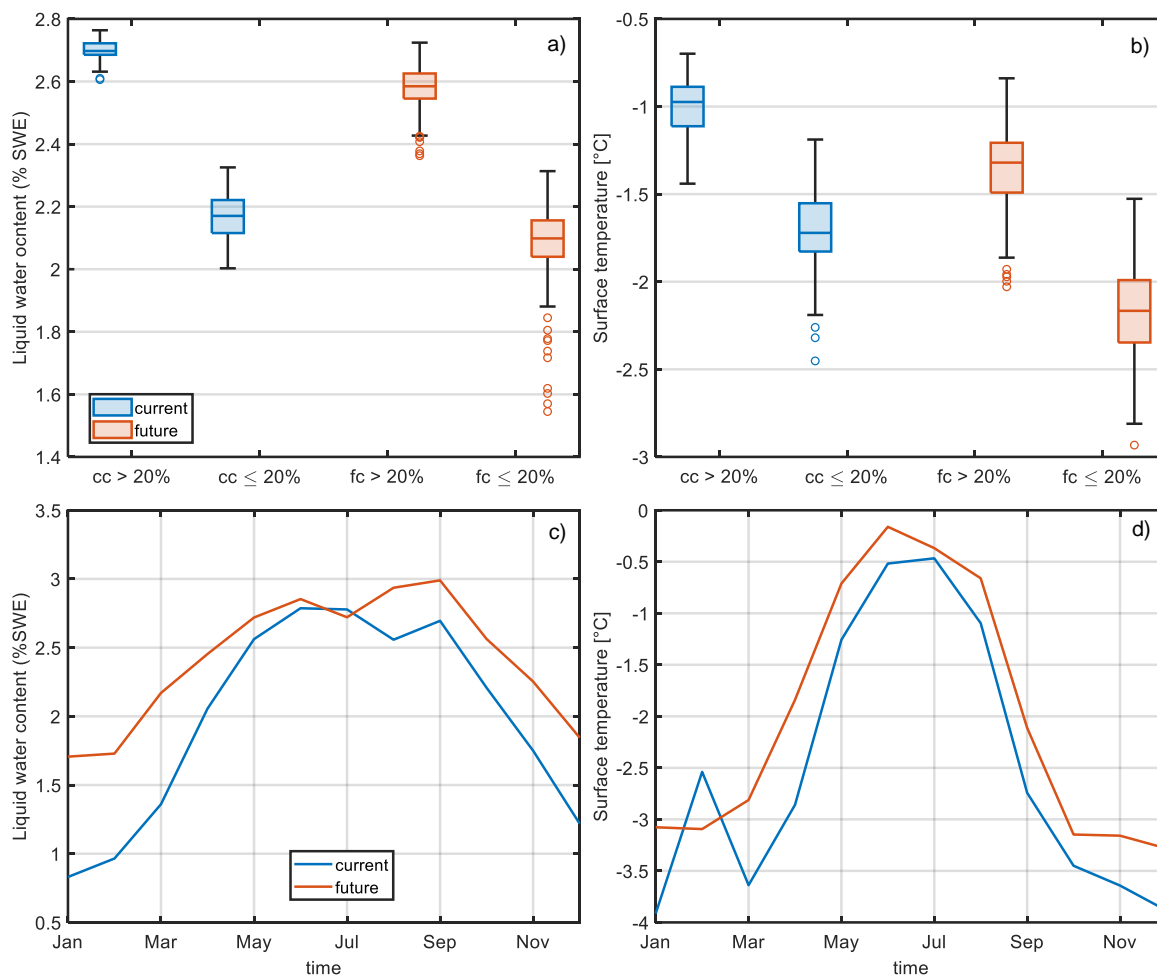
Figure 9. Climate period mean values of liquid water content in % SWE (a) and surface temperature of the snowpack (b) at the start of ROS events spatially averaged over pixel with snowmelt contributing more or less than 20% to SWI for current climate (cc) and future climate conditions (fc, RCP 8.5 at the end of the century). A contribution area >1/3 of the total area was chosen to define a ROS event and pixel-based criterion 2. In (c) and (d) monthly climate period mean values are shown for contribution area averages and pixel-based criterion 2. Values stemming from 50 (current climate) and 500 climate periods (future climate with 50 realizations of 10 climate models).

3.2.5 Rain-on-snow intensity and snowmelt contribution

Since rain intensity is expected to increase significantly in a future climate for all scenarios studied, also during ROS conditions (Fig. S2), one can expect SWI to increase for rain-on-snow events as well. However, the conclusions are very similar to those for ROS frequency. An increase of high SWI intensities is observable but is masked by the sources of uncertainty quantified in this study for all emission scenarios and time horizons (see Fig. S7 for RCP 4.5 at the end of the century) except for the most extreme scenario (Fig. 10), i.e. RCP 8.5 at the end of the century, still depending, however, on the ROS definition criteria. If the ROS criterion implies a substantial contribution of snowmelt to SWI, again, the increase is masked by uncertainty, whereas without this condition this is not the case. The elevation dependence is also very similar to the ROS frequency (not

shown): at higher elevations, the increase is pronounced for criteria 2 and 4 for elevations above 3000 m and 2500 m, respectively. For all other definitions of ROS events and all other emission scenarios and time horizons, this increase is also observed but is masked by sources of uncertainty.

385 Since snow cover decreases massively at the end of the century in the most extreme climate scenario RCP 8.5 (cp. Fig. 6d), it can be expected that the contribution of snowmelt to SWI also decreases and the observed increase in ROS events is mainly driven by an increase in rain intensity. However, this depends on the pixel-based definition of whether a positive or negative climate signal can be observed. When substantial snowmelt contributions are required, the signal is largely masked by sources of uncertainty (Fig. S8). These results show that despite a dramatic decrease in snowpack by the end of the century in an RCP 390 8.5 scenario, the role of snow in contributing to runoff does not largely change for ROS events.
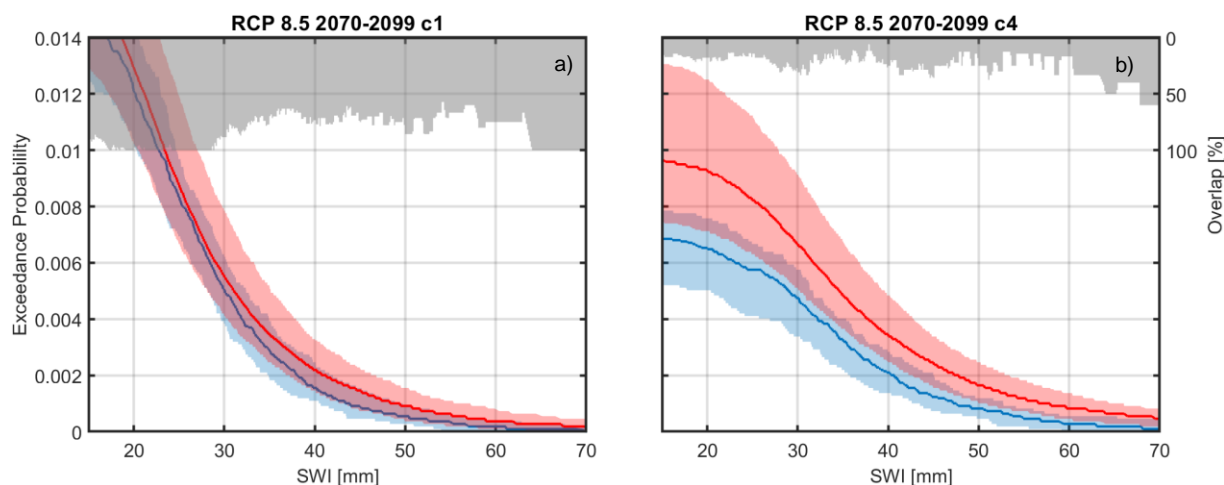
Figure 10. Yearly exceedance probability of total area-averaged SWI of ROS events for current climate (blue) and RCP 8.5 at the end of the century (red) for (a) criteria 1 (c1) and 4 (c4) (b). A contribution area >1/3 of the total area was chosen to define a ROS 395 **event. Plotted are the 5, 50, 95 percentiles of climate period mean values stemming from 50 (current climate) and 500 climate periods (future climate with 50 realizations of 10 climate models).**

3.2.6 Comparison with other studies

The results obtained here are based on a more complex approach than those of existing studies on this topic (e.g. Beniston and Stoffel, 2016; Morán-Tejeda et al., 2016; Musselman et al., 2018; Ohba and Kawese, 2020; Sezen et al., 2020), as we have 400 added two new dimensions, i.e. internal climate variability and the ROS definition. Beniston and Stoffel (2016) reported that in the Swiss Alps, an increase of nearly 50% in the number of ROS events occurred with 2-4 °C warmer temperatures than today at elevations of 2000 and 2500 m. For altitudes of 1500 m and below, a decrease in the number of ROS events was obtained. Except for two climate models, this temperature increase corresponds to the most extreme scenario RCP 8.5 at the end of the century (see Fig. 5a). Morán-Tejeda et al. (2016) came to very similar conclusions. Beniston and Stoffel (2016) and 405 Morán-Tejeda et al. (2016) did use, however, empirical snow models without the capability that water retention can depend on the state of the snowpack. Ohba and Kawase (2020) did not use snowmelt in their definition of ROS events and Sezen et

al. (2020) defined ROS events with a very small amount of snowmelt (0.1 mm d^{-1}). Thus, reporting more ROS events at high elevations is consistent with our results using a criterion that does not imply a substantial snowmelt contribution. We claim, however, that the ROS definition must account for the runoff perspective and should not be based only on the occurrence of
410   liquid precipitation on snowpack, because of the pronounced risk in flood potential due to excess runoff from snowmelt (Würzer et al., 2006). Thus, it is important to note that our results using ROS definitions, which require a substantial snowmelt contribution differ from existing studies, suggesting that more frequent rain on snow in the future does not result in a more frequent combination of rain and snowmelt, as highlighted in Section 3.2.4.

Musselman et al. (2018) defined ROS events identically to the criterion 1 chosen here (i.e. >10 mm rain per day, >10 mm
415   SWE, and >20% snowmelt contribution to SWI). They analyzed spatial energy balance model runs on a 4-km grid in western North America. Similar to the studies in Switzerland, they achieved a decrease in the number of ROS events at lower elevations and an increase at higher elevations for an RCP 8.5 emissions scenario by the end of the century, an increase of ROS intensity and a decrease in the contribution of snowmelt. These results can also be found in our study case, but they are largely obscured by sources of uncertainty (Figs. 10a and S8a). When natural climate variability is artificially suppressed in our analysis by
420   plotting only the first realization of a climate period (Fig. S9; note that the first realizations of the current and future climates are initialized with the same parameters in the weather generator), one can more clearly follow the conclusions of Musselman et al. (2018) of an increase in intensity and a decrease in snowmelt contribution.

In summary, similar conclusions compared to the cited literature would be drawn if our approach were simplified, i.e. (i) one does not distinguish between substantial and non-substantial snowmelt contribution based on snowpack conditions and/or (ii)
425   natural climate variability was not accounted for. This study shows that the inclusion of both natural climate variability and a snow model capable of modeling liquid water retention based on physical process representations provides new insights, particularly that only ROS events with no significant snowmelt contribution will occur more frequently in the future, while ROS events with significant snowmelt contribution will mainly shift towards earlier in the year.

3.2.7   Uncertainty partitioning

430   Figure 11 shows the relative contribution of the different sources of climate uncertainties for the climate change signal of seasonal SWE (ΔSWE) for the mid- and late-century. The total uncertainty at mid-century is split into two almost equal parts, total climate model uncertainty and total natural climate variability, while scenario uncertainty does not play a significant role. This changes for the end-of-century scenarios, for which the total uncertainty splits into roughly three equal parts. The larger role of scenario uncertainty at the end of the century was already visible in Fig. 6 and is mentioned by Verfaillie et al. (2018).
435   Verfaillie et al. (2018) also quantified snow model uncertainty and concluded that physical snow modeling has a contribution of up to 20% of the simulated results after mid-century, which they considered secondary to climate model spread. It was mentioned that its influence on trends (or climate change signals) is likely much smaller but was not quantified more precisely. This implies that natural climate variability is of much greater importance than physical snow model uncertainty, as it is of a comparable magnitude to climate model uncertainty.

440
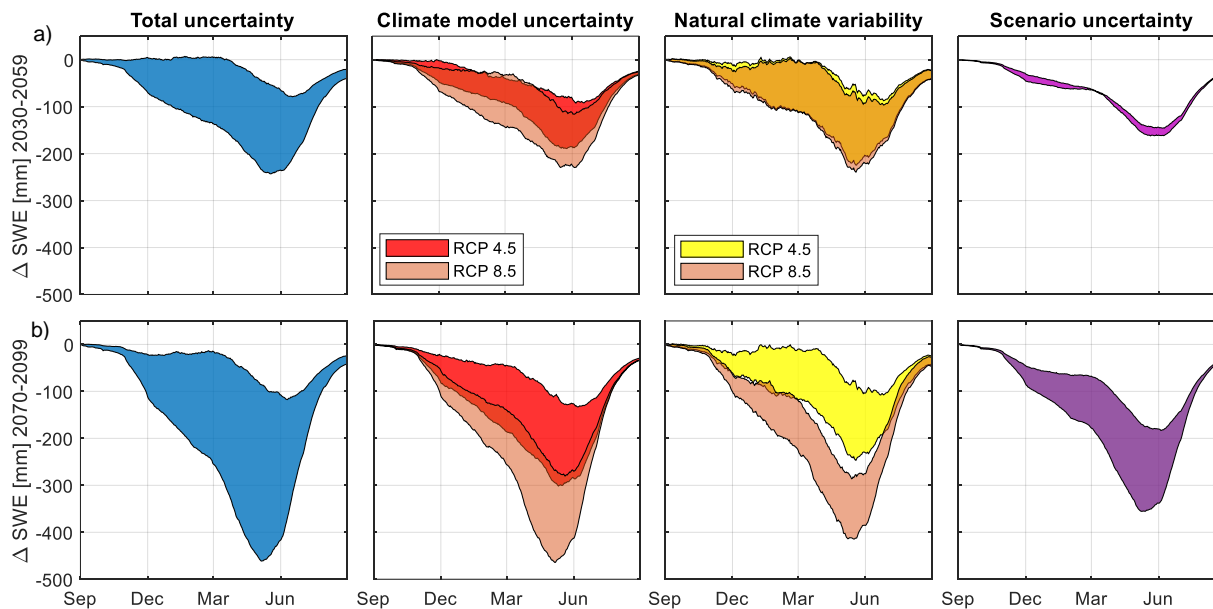
Figure 11. Uncertainty sources and their contribution to total uncertainty for seasonal climate change signal of SWE (ΔSWE) between current and future climate scenarios for mid (a) and (b) end of the century.

Fractional uncertainties were calculated for the SWE climate change signal as a weighted seasonal mean, using total
445 uncertainty values as weights (Fig. 12, SWE mean). Note that 5-95th percentile ranges are used here to quantify ranges of
fractional uncertainty (see Sect. 2.6), implying that the sum of ranges for (independent) random variables cannot be expected
to equal one. Mid-century natural climate variability has the largest contribution, accounting for more than 75% of the total
uncertainty range. At the end of the century, all sources of uncertainty are about equal in magnitude, consistently with the
visual evidence from Fig. 11. At the beginning and end of the snow season, natural climate variability has a larger relative
450 contribution than typically seen during the season (not shown), implying that for studies focusing on snow cover duration,
natural climate variability is particularly important. The increasing role of emissions scenario uncertainty in SWE projections
toward the end of the century implies that efforts to reduce uncertainties in snow forecasts should focus on constraining
uncertainties related to emission scenarios in a similar manner as efforts to improve climate models.

For the climate change signal of the ROS metrics studied here, natural climate variability is more important compared to
455 ΔSWE, in agreement with our initial hypothesis, because the frequency of future ROS events depends more on precipitation
and less on air temperature. Precipitation is more influenced by natural climate variability compared to air temperature at this
spatial scale (Fatichi et al., 2016; Peleg et al., 2019). For all ROS metrics, except for the annual exceedance probability of ROS
frequency using small spatial thresholds ("contribution area > 0.1"), natural climate variability dominates other sources of
uncertainty, with values between 70% and 95% of the total uncertainty range, even at the end of the century. In fact, the relative
460 contribution of the uncertainty sources of the ROS metrics studied here compares quite well on a local scale with the purely
precipitation-based metrics in Fatichi et al. (2016). This is in contrast to the continental scale studied in Hawkins and Sutton

(2011), where the role of natural climate variability in decadal mean precipitation diminishes and climate model uncertainty dominates toward the end of the century.

In summary, the total uncertainty in projections of the studied variables is composed of natural climate variability, climate
465 model uncertainty, and emission scenario uncertainty, in this order for SWE projections only up to mid-century, and for all other variables up to the end of the century. The large contribution of natural climate variability demonstrates the need to quantify this source of uncertainty to prevent avoidable biases by end-users and decision-makers.
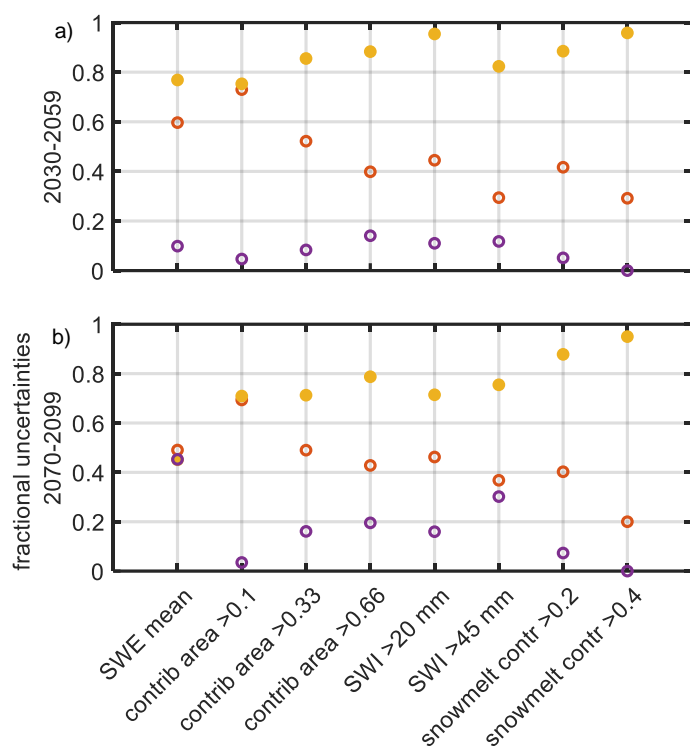
470 **Figure 12. Fractional uncertainties of total climate model uncertainty (red), total natural variability (yellow) and emission scenario uncertainty (purple) for the mid (a) and the end of the century (b). 'SWE mean' is a weighted seasonal average taking the total uncertainty as weights, 'contrib area' is the contribution area defined with criterion 2 for two thresholds (cp. Fig. 7), 'SWI' is the Surface Water Input (cp. Fig. 10) and 'snowmelt contr' is the snowmelt contribution in % of SWI (cp. Fig. S8).**

4   Conclusions

475 The climate change signal of snow water resources and of ROS frequency and intensity was investigated with their climatic uncertainties. For the exemplary selected high-altitude study area in the Swiss Alps, the climate change signal towards fewer snow water resources during the ablation period was found to emerge clearly from the sources of uncertainty for all scenarios investigated. However, given significant uncertainties, there is some overlap during the accumulation period for all but the most extreme scenario (RCP 8.5, end of the century).

480   For ROS events, previous studies have shown that they will become more frequent and intense at higher elevations due to a shift toward liquid precipitation and despite a decreasing snowpack. The additional inclusion of natural climate variability in the uncertainty assessment revealed that this source is responsible for 70-90% of the overall uncertainty, similar to purely precipitation-based metrics. As a result, for all scenarios, including RCP 8.5 at the end of the century, the climate change signal of ROS frequency and intensity is larger than the uncertainty range only for events with no significant contribution of snowmelt

485   to runoff (<20%). For events with a significant contribution of snowmelt to runoff, the climate change signal is too small and could potentially only be explained by natural climate variability. These events regularly occur during conditions with an initial warm and wet snowpack. The very rapid decline in snowpack toward early summer in future climate, when conditions typically prevail for substantial contributions from snowmelt, will result in a large decrease in such ROS events that cannot be compensated for at other times of the year: in early and midwinter, when rain is expected to fall more often in a future climate,

490   it will fall on snow that will be typically too cold and too dry to allow a significant contribution from snowmelt. Warmer air temperatures due to a changing climate are more likely to change the phase of precipitation than the condition of the snowpack to contribute significantly to runoff. This implies that ROS events with a significant contribution of snowmelt to runoff will occur earlier in the year, but not more frequent under future climate.

These additional results were possible only with increased model complexity, first by using a snow model that represents water

495   retention in snow-based on physical processes, and second by accounting for natural climate variability to quantify the signal-to-noise ratio of climate at the local scale. Natural climate variability, climate model uncertainty, and emission scenario uncertainty, in this order, composed the total uncertainty for SWE projections up to mid-century, and for ROS projections up to the end of the century. Therefore, it is vital to quantify natural climate variability in snow projections in order to avoid bias among end-users and decision-makers.

500 **5   Data availability**

Daily data of simulated current and future climate periods are available at (https://www.envidat.ch/#/metadata/multiple-realizations-of-daily-swe-swi-and-rain-projections). This is a preliminary dataset, as the review process of the associated manuscript has not yet been completed. Once the final version of the manuscript is published, the dataset will be assigned a DOI.

505 **6   Author contribution**

MS led the project, created and verified the modeled data set, analyzed the data, and wrote the manuscript. NP set up and trained the weather generator, verified the modeled data and discussed the results. AW worked on the snow model and discussed the results. TJ provided ideas for data analysis and discussed results. TJ, PB and NP contributed to the writing and editing of the manuscript.

510 **7   Competing interests**

The authors declare that they have no conflict of interest.

8   Acknowledgments

MS would like to thank Thomas Kramer for HPC computing support and Louis Queno and Nora Helbig for the continued development of the snow model. He would also like to thank Massimiliano Zappa for providing funding to complete the
515 manuscript. MS and NP were partly funded by the Swiss Competence Center for Energy Research-Supply of Electricity (http://www.sccer-soe.ch).

9   References

Addor, N., Rössler, O., Köplin, N., Huss, M., Weingartner, R., and Seibert, J.: Robust changes and sources of uncertainty in the projected hydrological regimes of Swiss catchments. Water Resources Research, 50(10), 7541-7562,
520   https://doi.org/10.1002/2014WR015549, 2014.

Anandhi, A., Frei, A., Pierson, D. C., Schneiderman, E. M., Zion, M. S., Lounsbury, D., and Matonse, A. H.: Examination of change factor methodologies for climate change impact assessment, Water Resources Research, 47, W03501, doi:10.1029/2010WR009104, 2011.

Beniston, M., and Stoffel, M.: Rain-on-snow events, floods and climate change in the Alps: Events may increase with
525   warming up to 4 C and decrease thereafter. Science of the Total Environment, 571, 228-236, https://doi.org/10.1016/j.scitotenv.2016.07.146, 2016.

CH2018 Project Team: CH2018 - Climate Scenarios for Switzerland. National Centre for Climate Services. doi:10.18751/Climate/Scenarios/CH2018/1.0, 2018.

Clark, M. P., Wilby, R. L., Gutmann, E. D., Vano, J. A., Gangopadhyay, S., Wood, A. W., Fowler, H.J., Prudhomme, Ch.,
530   Arnold, J.R. and Brekke, L. D.: Characterizing uncertainty of the hydrologic impacts of climate change. Current Climate Change Reports, 2(2), 55-64, https://doi.org/10.1007/s40641-016-0034-x, 2016.

Deser, C., Knutti, R., Solomon, S., and Phillips, A.S.: Communication of the role of natural variability in future North American climate. Nature Climate Change, 2, 775, https://doi.org/10.1038/nclimate1562, 2012a.

Deser, C., Phillips, A., Bourdette, V., and Teng, H.: Uncertainty in climate change projections: the role of internal
535   variability. Climate dynamics, 38(3), 527-546, https://doi.org/10.1007/s00382-010-0977-x, 2012b.

Essery, R., Morin, S., Lejeune, Y., and Ménard, C. B.: A comparison of 1701 snow models using observations from an alpine site. Advances in water resources, 55, 131-148, https://doi.org/10.1002/2014WR016498, 2014.

Fatichi, S., Rimkus, S., Burlando, P., and Bordoy, R.: Does internal climate variability overwhelm climate change signals in streamflow? The upper Po and Rhone basin case studies. Science of the Total Environment, 493, 1171-1182,
540   https://doi.org/10.1016/j.scitotenv.2013.12.014, 2014.

Fatichi, S., Ivanov, V.Y., Paschalis, A., Peleg, N., Molnar, P., Rimkus, S., Kim, J., Burlando, P. and Caporali, E.: Uncertainty partition challenges the predictability of vital details of climate change. Earth's Future, 4, 240-251, https://doi.org/10.1002/2015EF000336, 2016.

Ghil, M.: Natural climate variability. Encyclopedia of global environmental change, 1, 544-549, 2002.

545   Griessinger, N., Schirmer, M., Helbig, N., Winstral, A., Michel, A., and Jonas, T.: Implications of observation-enhanced energy-balance snowmelt simulations for runoff modeling of Alpine catchments. Advances in Water Resources, 133, 103410, https://doi.org/10.1016/j.advwatres.2019.103410, 2019.

Hawkins, E., and Sutton, R.: The potential to narrow uncertainty in regional climate predictions. Bulletin of the American Meteorological Society, 90(8), 1095-1108, https://doi.org/10.1007/s00382-010-0810-6, 2009.

550   Hawkins, E., and Sutton, R.: The potential to narrow uncertainty in projections of regional precipitation change. Climate dynamics, 37(1), 407-418, https://doi.org/10.1175/2009BAMS2607.1, 2011.

Helbig, N., Van Herwijnen, A., Magnusson, J., and Jonas, T.: Fractional snow-covered area parameterization over complex topography. Hydrology and Earth System Sciences, 19(3), 1339-1351, https://doi.org/10.5194/hess-19-1339-2015, 2015.

555   Helbig, N., Schirmer, M., Magnusson, J., Mäder, F., van Herwijnen, A., Quéno, L., Bühler, Y., Deems, J. S., and Gascoin, S.: A seasonal algorithm of the snow-covered area fraction for mountainous terrain, The Cryosphere Discuss. [preprint], https://doi.org/10.5194/tc-2020-377, accepted for final publication, 2021.

Jacob, D., Petersen, J., Eggert, B. et al.: EURO-CORDEX: new high-resolution climate change projections for European impact research. Reg Environ Change, 14, 563–578, https://doi.org/10.1007/s10113-013-0499-2, 2014.

560   Lafaysse, M., Hingray, B., Mezghani, A., Gailhard, J., and Terray, L.: Internal variability and model uncertainty components in future hydrometeorological projections: The Alpine Durance basin. Water resources research, 50(4), 3317-3341, https://doi.org/10.1002/2013WR014897, 2014.

Magnusson, J., Gustafsson, D., Hüsler, F., and Jonas, T.: Assimilation of point SWE data into a distributed snow cover model comparing two contrasting methods. Water resources research, 50(10), 7816-7835,
565   https://doi.org/10.1002/2014WR015302, 2014.

Magnusson, J., Wever, N., Essery, R., Helbig, N., Winstral, A., and Jonas, T.: Evaluating snow models with varying process representations for hydrological applications. Water Resources Research, 51(4), 2707-2723, https://doi.org/10.1002/2014WR016498, 2015.

Marty, C., Schlögl, S., Bavay, M., and Lehning, M.: How much can we save? Impact of different emission scenarios on
570   future snow cover in the Alps, The Cryosphere, 11, 517–529, https://doi.org/10.5194/tc-11-517-2017, 2017.

MeteoSwiss, https://www.meteoswiss.admin.ch/content/dam/meteoswiss/de/service-und-publikationen/produkt/raeumliche-daten-niederschlag/doc/ProdDoc_RhiresD.pdf, 2019.

Moraga, J.S., Peleg, N., Fatichi, S., Molnar, P., and Burlando, P.: Revealing the impacts of climate change on mountainous catchments through high-resolution modelling. Journal of Hydrology, https://doi.org/10.1016/j.jhydrol.2021.126806, 2021.

Morán-Tejeda, E., López-Moreno, J. I., Stoffel, M., and Beniston, M.: Rain-on-snow events in Switzerland: recent observations and projections for the 21st century. Climate Research, 71(2), 111-125, https://doi.org/10.3354/cr01435, 2016.

Musselman, K. N., Clark, M. P., Liu, C., Ikeda, K., and Rasmussen, R.: Slower snowmelt in a warmer world. Nature Climate Change, 7(3), 214-219, https://doi.org/10.1038/nclimate3225, 2017.

Musselman, K.N., Lehner, F., Ikeda, K., Clark, M.P., Prein, A.F., Liu C., Barlage, M. and Rasmussen, R.: Projected increases and shifts in rain-on-snow flood risk over western North America. Nature Clim Change **8,** 808–812, https://doi.org/10.1038/s41558-018-0236-4, 2018.

Ohba, M., and Kawase, H.: Rain-on-Snow events in Japan as projected by a large ensemble of regional climate simulations. Clim Dyn 55, 2785–2800, https://doi.org/10.1007/s00382-020-05419-8, 2020.

Peleg, N., Fatichi, S., Paschalis, A., Molnar, P., and Burlando, P.: An advanced stochastic weather generator for simulating 2-D high-resolution climate variables. Journal of Advances in Modeling Earth Systems, 9(3), 1595-1627, https://doi.org/10.1002/2016MS000854, 2017.

Peleg, N., Molnar, P., Burlando, P., and Fatichi, S.: Exploring stochastic climate uncertainty in space and time using a gridded hourly weather generator. Journal of Hydrology, 571, 627-641, https://doi.org/10.1016/j.jhydrol.2019.02.010, 2019.

Schwarb, M.: The Alpine precipitation climate: evaluation of a high-resolution analysis scheme using comprehensive rain-gauge data (Doctoral dissertation, ETH Zurich), https://doi.org/10.3929/ethz-a-004121274, 2000.

Sezen, C.; Šraj, M.; Medved, A.; Bezak, N. Investigation of Rain-On-Snow Floods under Climate Change. Appl. Sci., 10, 1242, https://doi.org/10.3390/app10041242, 2020.

Surfleet, C. G., & Tullos, D., 2013. Variability in effect of climate change on rain-on-snow peak flow events in a temperate climate. Journal of Hydrology, 479, 24-34, https://doi.org/10.1016/j.jhydrol.2012.11.021, 2013.

Verfaillie, D., Lafaysse, M., Déqué, M., Eckert, N., Lejeune, Y., and Morin, S.: Multi-component ensembles of future meteorological and natural snow conditions for 1500 m altitude in the Chartreuse mountain range, Northern French Alps, The Cryosphere, 12, 1249–1271, https://doi.org/10.5194/tc-12-1249-2018, 2018.

Willibald, F., Kotlarski, S., Grêt-Regamey, A., and Ludwig, R.: Anthropogenic climate change versus internal climate variability: impacts on snow cover in the Swiss Alps, The Cryosphere, 14, 2909–2924, https://doi.org/10.5194/tc-14-2909-2020, 2020.

Winstral, A., Jonas, T., and Helbig, N.: Statistical downscaling of gridded wind speed data using local topography. Journal
605   of Hydrometeorology, 18(2), 335-348, https://doi.org/10.1175/JHM-D-16-0054.1s, 2017.

Winstral, A., Magnusson, J., Schirmer, M., and Jonas, T.: The bias-detecting ensemble: A new and efficient technique for
     dynamically incorporating observations into physics-based, multilayer snow models. Water Resources Research, 55(1),
     613-631, https://doi.org/10.1029/2018WR024521, 2019.

Würzer, S., Jonas, T., Wever, N., and Lehning, M.: Influence of initial snowpack properties on runoff formation during rain-
610   on-snow events. Journal of hydrometeorology, 17(6), 1801-1815, https://doi.org/10.1175/JHM-D-15-0181.1, 2016.